Comparison of phenomenological and fundamental modelling approaches for predicting fluidized bed reactor performance

Schalk Cloete[1], Abdelghafour Zaabout[2], Stein Tore Johansen[2] & Shahriar Amini[2*]

[1] NTNU Department of Energy and Process technology, Trondheim, NORWAY

[2] SINTEF Materials and Chemistry, Trondheim, NORWAY

*Corresponding author: shahriar.amini@sintef.no

Keywords: Computational fluid dynamics; Phenomenological model; 1D Model; Fluidized bed reactor; Kinetic theory of granular flows; Central composite design.

1 Abstract

Two approaches to modelling fluidized bed reactors were evaluated and compared in this work: a phenomenological 1D approach based on empirical closures and a more fundamental 2D approach based on computational fluid dynamics (CFD). The fundamental modelling approach should be more accurate and generic, but is several orders of magnitude more computationally expensive than the phenomenological approach. Therefore, the development of accurate, but computationally affordable phenomenological models is a matter of great importance. This work evaluated the behaviour of both modelling approaches over a wide range of operating variables spanning the bubbling fluidization regime. These variables included fluidization velocity, bed height, operating temperature and particle size. Several different closure models were evaluated for the phenomenological approach and it was shown that models for the bubble size, bubble-to-

emulsion mass transfer coefficient and solids inside the bubble all have a significant impact on model performance. An optimal combination of closure models used in the phenomenological approach succeeded in providing a good match to data gathered from the more generic fundamental approach. The response of the model to changes in particle size was identified as the area with the greatest potential for further development. More detailed comparisons of axial distributions of important flow variables showed some differences between the predictions of the phenomenological and fundamental modelling approaches. In particular, the hydrodynamic measures of axial void distribution and bubble rise velocity predicted by these two approaches showed some significant differences.

2 Nomenclature

2.1 Main Symbol definitions:

Greek symbols:

α	Volume fraction
δ	Bubble fraction
ε	Void fraction
ϕ	Kinetic energy transfer rate (kg/m.s^3)
γ	Dissipation rate (kg/m.s^3)
μ	Viscosity (kg/m.s)
Θ_s	Granular temperature (m^2/s^2)
ρ	Density (kg/m^2)
ς	Specularity coefficient
$\bar{\bar{\tau}}$	Stress tensor (kg/m.s^2)

$\vec{\tau}_s$ Particle shear force at the wall (N)

$\vec{\upsilon}$ Velocity vector (m/s)

∇ Del operator / Gradient (1/m)

Ar Archimedes number

C Molar concentration (mol/m^3)

D Diffusivity (m^2/s)

d Diameter (m)

g Gravitational constant (9.81 m/s)

$\vec{g}$ Gravity vector (m/s^2)

$g_{0,ss}$ Radial distribution function

H Bed height (m)

h Height within the reactor (m)

$\overline{\overline{I}}$ Identity tensor

$\vec{J}$ Diffusive flux (kg/(m^2.s))

K Momentum exchange coefficient (kg/(m^3.s)

K Mass transfer coefficient (1/s)

k Diffusion coefficient (kg/m.s)

k Reaction rate constant (m/s)

M Molar mass (kg/mol)

N Moles (mol)

p Pressure (Pa)

R Gas constant (8.314 J/K.mol)

R^H Heterogeneous reaction rate (mol/m^{3}s)

S Source term (kg/m^{3}s)

T Temperature (K)

t Time (s)

U Velocity (m/s)

$\vec{U}_{s,\parallel}$ Particle velocity parallel to wall (m/s)

V Volume (m^3)

x Mass fraction

Y Species mass fraction

z Axial distance (m)

2.2 Sub- and superscript definitions:

0 Inlet

Θ_s Granular temperature

A Species A

b Bubble

br Bubble rise

c Cloud or core

e Emulsion

ex Expanded bed

g Gas or grain

gs Inter-phase

i Species index

max Maximum packing

mf Minimum fluidization

n	Reaction order
p	Particle
s	Solids
st	Static

2.3 Abbreviations

by	Interaction effect
d	Particle diameter
H	Initial static bed height
L	Linear effect
Q	Quadratic effect
SS	Sum of squares
T	Temperature
U	Fluidization velocity

3 Introduction

Modelling of non-linear systems such as fluidized bed reactors is essential for the purposes of optimization, control and scale-up. Various hydrodynamic models have been presented in the literature in order to address this need. Initially, simple contacting models such as plug flow, mixed flow and tanks in series were tested [1]. However, a major advance seen in fluidized bed reactor modelling was the introduction of two-phase theory [2]. According to this theory, the fluidized bed consists of two phases; the emulsion phase where the gas is flowing under minimum fluidization conditions through a dense mass of solids and the bubble phase where no solids are present and the gas can rise at velocities significantly greater than the fluidization velocity. Subsequently, the existence of a third phase in the form of a particle cloud between the

bubble and the emulsion phases was also considered [3], especially for beds with fine particles. This cloud phase was neglected for intermediate and coarse particles though. Over the following decades many models were developed for industrial fluidized beds on the basis of this theory [4, 5]. Models were developed for gas-solid catalytic cracking [6, 7] and for heterogeneous gas-solid reactions [8, 9] and were shown to give adequate predictions of process performance.

Despite its success, the simple two phase model (STP) has received criticism for under-predictions of reactor performance because of two inaccurate assumptions: (i) the bubble is free of solids and (ii) the emulsion phase is under minimum fluidization conditions. Alternative approaches were proposed to address these assumptions [10, 11]. In addition, the two-phase model was also extended from its basis in bubbling fluidization to the regimes of turbulent [12] and the fast fluidization [13].

Even though such extensions are available, the simple two-phase model (STP) is best applied in the bubbling fluidization regime for which it was originally developed. Even so, the success of the models largely depends on accurate closure laws for the bubble size and the inter-phase mass transfer. Considering the existence of solids inside the bubble may also be necessary to improve model performance.

Several formulations of the bubble size and the mass transfer coefficient are available in the literature, but a clear consensus on the best performing model combination is yet to be reached. Assessment of model performance with respect to different formulations of various constituent models over a wide range of operating conditions covering the bubbling regime is therefore of high importance. For this reason, the response of model performance to changes in four independent variables (fluidization velocity, static bed height, particle size, and temperature) is studied in this work.

Computational fluid dynamic (CFD) modelling based on the standard two fluid model closed by the kinetic theory of granular flows (KTGF) [14-16] was chosen to assess 1D model performance. This methodology has been used extensively in the published literature over the past three decades and has been hydrodynamically validated (e.g. [17]). CFD also offers great flexibility to investigate the effects of changes in any conceivable independent variable and is therefore an ideal tool to use in the present study where a wide range of independent variables will be investigated. Physical experimentation over such a wide range of variables would be prohibitively complex and expensive.

4 Simulations

Both phenomenological 1D and fundamental 2D simulations were performed and compared in this work. The theoretical bases behind these approaches will be presented separately below.

4.1 1D model theory

The simple two phase model (STP) was used as a basis for the 1D modelling conducted in this study. Several additions were made to the STP in its standard form.

4.1.1 Standard STP model equations

The fluidized bed is assumed to consist of two phases; the particle-rich emulsion phase and the particle-lean bubble phase. The STP model assumes that the bubbles are solid-free and reactions occur only in the emulsion phase where the gas flows upwards at minimum fluidization velocity. The equation system solved in this modelling approach is given in Table 1. This combination of closure relations were chosen based on their popularity in the open literature and successful comparisons to experimental data [9, 11].

Table 1: Model equations used in the 1D approach.

Mole balances for species i in the bubble and emulsion phases	$U_b \frac{dC_{bi}}{dz} + K_{be}(C_{bi} - C_{ei}) + R^H = 0$	**Equation 1**
	$U_{mf}(1-\delta)\frac{dC_{ei}}{dz} - K_{be}\delta(C_{bi} - C_{ei}) + (1-\delta)R^H = 0$	**Equation 2**
Bubble fraction	$\delta = \frac{U_0 - U_{mf}}{U_b - U_{mf}}$	**Equation 3**
Minimum fluidization velocity [18]	$\frac{U_{mf}\rho_g d_p}{\mu_g} = \sqrt{27.2^2 + 0.0408Ar} - 27.2$	**Equation 4**
Void at minimum fluidization [18]	$\varepsilon_{mf} = 0.586Ar^{-0.029}(\rho_g / \rho_s)^{0.021}$	**Equation 5**
Bubble diameter [19] (Equation 6)	$d_b = 0.21h^{0.8}(U_0 - U_{mf})^{0.42}\exp[-0.25(U_0 - U_{mf})^2 - 0.1(U_0 - U_{mf})]$	**Equation 6**
[20] (Equation 7)	$d_b = 0.54(U_0 - U_{mf})^{0.4}(h + 4\sqrt{A_0})^{0.8} g^{-0.2}$	**Equation 7**
Bubble velocity [2]	$U_b = U_0 - U_{mf} + U_{br}$	**Equation 8**
Bubble rise velocity [2]	$U_{br} = 0.711\sqrt{gd_b}$	**Equation 9**
Bubble to emulsion mass transfer coefficient	$\frac{1}{K_{be}} = \frac{1}{K_{bc}} + \frac{1}{K_{ce}}$	**Equation 10**
[3] (Equation 10)	$K_{bc} = 4.5\left(\frac{U}{d_b}\right) + 5.85\left(\frac{D_g^{1/2}.g^{1/4}}{d_b^{5/4}}\right)$	**Equation 11**

[21] (Equation 13)	$K_{ce} = 6.77\left(\frac{D_g \varepsilon_e U_{br}}{d_b^3}\right)^{1/2}$	**Equation 12**
	$K_{be} = \frac{1}{d_b}\left(2U_{mf} + 12\left(\frac{D_g \varepsilon_{mf} U_b}{\pi d_b}\right)^{0.5}\right)$	**Equation 13**
Mean bed void	$\varepsilon = (1-\delta)\varepsilon_{mf} + \delta\varepsilon_b$	**Equation 14**
Expanded bed height	$H_{ex} = \frac{0.6H_{st}}{1-\varepsilon}$	**Equation 15**

4.1.2 Model enhancements and alternative formulations

Equation 7 and the Equation 11 were used for the bubble size and mass transfer in initial 1D simulations. Alternative model formulations were subsequently evaluated in the form of Equation 6 for the bubble size as well as variations on Equation 10 and its constituents and Equation 13 for the mass transfer. The best performing model combinations were retained for any subsequent simulations.

The STP formulation was also improved by considering the existence of solid particles inside the bubble. A simple initial model was derived from CFD for this purpose.

4.1.3 Solution strategy

The system of equations given in Table 1 was solved using an algorithm implemented in MATLAB. The entire reactor was divided into constant sections with a height of Δz. Hydrodynamic parameters (bubble size and velocity, the mass transfer coefficient, etc.) were determined in each section, after which the mole balance equations were solved to get the axial species concentration. A Runge-Kutta method was used to solve the mole balance equations

sequentially at each section along the height of the reactor. Once the species concentrations were determined, the overall gas conversion could be calculated.

An iterative method was used to calculate the expanded bed height, by evaluating it (Equation 15) at each reactor section on the basis of the mean bed void from this section downwards. The difference between the calculated expanded bed height and the level of height at which it was evaluated was calculated at each level and convergence was assumed when this difference became smaller than Δz.

4.2 2D model theory

The fundamental modelling in this study was done within the framework of computational fluid dynamics (CFD). The well-known two fluid model (TFM) closed by the kinetic theory of granular flows (KTGF) was used as the basis for the calculations.

4.2.1 Model equations

The conservation equations are solved for each of the two phases present in the simulation. The continuity equations for the gas and solids phases are given below:

$$\frac{\partial}{\partial t}\left(\alpha_g \rho_g\right) + \nabla \cdot \left(\alpha_g \rho_g \vec{\upsilon}_g\right) = 0 \qquad \textbf{Equation 16}$$

$$\frac{\partial}{\partial t}\left(\alpha_s \rho_s\right) + \nabla \cdot \left(\alpha_s \rho_s \vec{\upsilon}_s\right) = 0 \qquad \textbf{Equation 17}$$

The conservation of momentum for the gas phase is written as follows:

$$\frac{\partial}{\partial t}\left(\alpha_g \rho_g \vec{\upsilon}_g\right) + \nabla \cdot \left(\alpha_g \rho_g \vec{\upsilon}_g \vec{\upsilon}_g\right) = -\alpha_g \nabla p + \nabla \cdot \bar{\bar{\tau}}_g + \alpha_g \rho_g \vec{g} + K_{sg}\left(\vec{\upsilon}_s - \vec{\upsilon}_g\right) \qquad \textbf{Equation 18}$$

And for the solids as:

$$\frac{\partial}{\partial t}\left(\alpha_s \rho_s \vec{\upsilon}_s\right) + \nabla \cdot \left(\alpha_s \rho_s \vec{\upsilon}_s \vec{\upsilon}_s\right) = -\alpha_s \nabla p - \nabla p_s + \nabla \cdot \bar{\bar{\tau}}_s + \alpha_s \rho_s \vec{g} + K_{gs}\left(\vec{\upsilon}_g - \vec{\upsilon}_s\right) \qquad \textbf{Equation 19}$$

The inter-phase momentum exchange coefficient $\left(K_{gs} = K_{sg}\right)$ was modelled according to the formulation of Syamlal and O'Brian [16].

Species are also conserved for the gas phase.

$$\frac{\partial}{\partial t}\left(\alpha_g \rho_g Y_{gi}\right) + \nabla \cdot \left(\alpha_g \rho_g \vec{\upsilon}_g Y_{gi}\right) = \nabla \cdot \alpha_g \vec{J}_{gi} + \alpha_g S_{gi} \qquad \textbf{Equation 20}$$

No energy conservation was included under the assumption of isothermal flow. This is usually a good assumption due to the excellent mixing achieved in fluidized bed reactors.

The KTGF [14-16] was implemented to model solids stresses resulting from particle collisions and uncorrelated translations. Kinetic energy contained in the random particle motions is quantified in terms of granular temperature and can be written in conservation form as follows:

$$\frac{3}{2}\left[\frac{\partial}{\partial t}\left(\alpha_s \rho_s \Theta_s\right) + \nabla \cdot \left(\alpha_s \rho_s \vec{\upsilon}_s \Theta_s\right)\right] = \left(-p_s \bar{\bar{I}} + \bar{\bar{\tau}}_s\right) : \nabla \vec{\upsilon}_s + \nabla \cdot \left(k_{\Theta_s} \nabla \Theta_s\right) - \gamma_{\Theta_s} + \phi_{gs} \qquad \textbf{Equation 21}$$

In the present study, this equation was solved in its algebraic form by neglecting the contributions of convection and diffusion. This is a good assumption in dense and slow moving bubbling beds since the local generation and dissipation strongly outweighs contributions from convective and diffusive fluxes. Equation 21 is therefore solved algebraically based on the local balance of granular temperature generation due to solids stresses and dissipation due to inelastic collisions [15] and damping by the primary phase [14].

The granular temperature is subsequently used to calculate values of the solids viscosity which is used in the solids stress tensor. Bulk viscosity [15] and the three components of shear viscosity, collisional [14, 16], kinetic [14] and frictional [22], were considered in the calculations.

Normal stresses modelled according to the solids pressure used in Equation 19 as well as in Equation 21 is calculated according to Lun *et al.* [15]. The radial distribution function which is a measure of the average distance between particles is a central concept in the KTGF and is calculated according to Ogawa and Oshima [23].

4.2.2 Flow solver and solver settings

The commercial software package, FLUENT 13.0 was used as the solver. The phase coupled SIMPLE scheme [24] was used for pressure-velocity coupling and the higher order QUICK scheme [25] for the spatial discretization of all remaining equations. First order implicit temporal discretization was used.

4.2.3 Geometry and meshing

A 2D plane geometry, 0.28 m in width and 2 m in high, was used to simulate the fluidized bed. The bed dimensions and flow conditions were based on a validated simulation experiment [17] in order to increase confidence in model results. The geometry was divided into two zones: the bed zone with a height of 1.8 m and a porous zone for the remaining 0.2 m. The porous zone was specified at the top of the freeboard in order to achieve a plug flow and prevent any backflow occurring at the outlet.

The domain was meshed with structured, 5 mm cells and continuously adaptively refined to 2.5 mm in the regions of the gas-emulsion interface as illustrated in Figure 1. The interface was identified as regions exhibiting high solids volume fraction gradients. The mesh adaptation was carried out every second timestep.

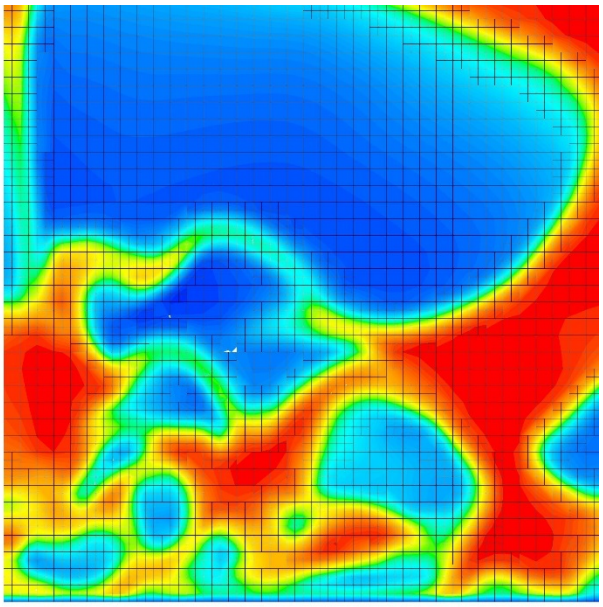

Figure 1: Snapshot of the contours of solids volume fraction near the bottom left corner of the bed illustrating the adaptive mesh refinement used in this study. Note the fine mesh on the gas-solid interface.

This technique was found to enable a significant decrease in cell count without compromising accuracy as illustrated in Figure 2. Aside from one point which displayed about a 10% difference for unknown reasons, the dynamically adapted grid predicted close to identical reactor performance. It can be seen that grid independence is achieved at a grid size of roughly 3.5 mm. The 2.5 mm grid was selected as a conservative measure because the simulations would be carried out over a wide range of operating conditions which might have an effect on grid independence and because computational demands with this grid size were still acceptable.

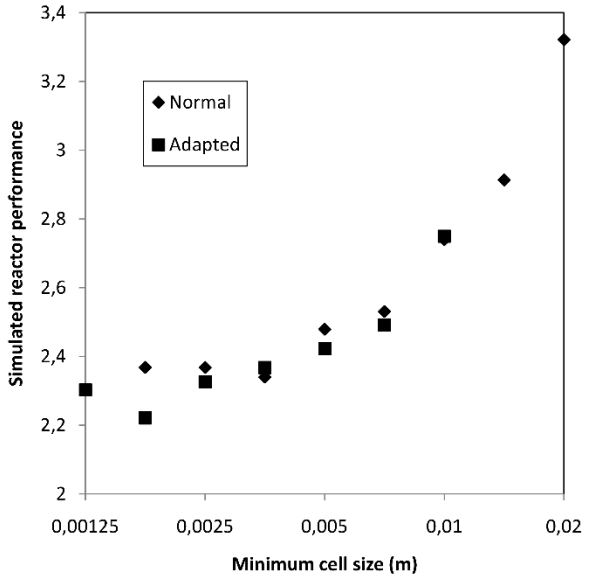

Figure 2: The sensitivity of the overall reactor performance (-log(x_A) at the outlet) to changes in the mesh size. The adapted grid size represent the size of the refined cells.

4.2.4 Boundary Conditions

At the two side boundaries of the simple rectangular domain, a simple no-slip wall boundary condition was set for the gas phase. The Johnson and Jackson [26] boundary condition was used for the granular phase with a specularity coefficient (ς) of 0.5.

$$\vec{\tau}_s = -\frac{\pi}{6}\sqrt{3}\varsigma\frac{\alpha_s}{\alpha_{s,\max}}\rho_s g_{0,ss}\sqrt{\Theta_s}\vec{U}_{s,\|} \qquad \textbf{Equation 22}$$

This value was found to give the best comparison to the experimental data of Taghipour *et al.* [17] on which the current simulated geometry is based. At the bottom boundary, a velocity inlet condition was implemented to inject gas at a velocity as specified by the specific simulation run in question. The injected gas consisted of pure reactant. The outlet at the top boundary of the domain was specified as a pressure outlet at atmospheric pressure.

4.2.5 Simulation summary

A summary of the physical properties and simulation parameters are given in Table 2.

Table 2: Physical properties and simulation parameters

Gas density (A and B)	0.3 kg/m^3
Gas viscosity (A and B)	3x10^{-5} kg/m·s
Particle density	2500 kg/m^3
Grain diameter	1 μm
Bed width	0.28 m
Bed height	2 m
Particle-particle restitution	0.9
Specularity coefficient	0.5
Initial solids packing	0.60
Maximum packaging limit	0.63
Mesh size	5 mm adaptively refined to 2.5 mm
Time step size	4e-4 to 8e-4 s

4.3 Reaction kinetics description

Reaction kinetics were implemented using the shrinking core model [27] with reaction rate as the limiting step. A simple, catalytic conversion of gas species A to gas species B was simulated to occur on the surface of microscopic solid grains (*S*) within the particles used in the fluidized bed:

$$A + S \rightarrow B + S$$

The physical properties of species A and B were specified to be identical (Table 2) so that the reaction would not influence the hydrodynamics resulting in a non-linear interaction. This will significantly simplify the interpretation of results.

When reaction rate control is assumed with the shrinking core model, the rate of consumption of species A on the surface of the unreacted core can be expressed as follows:

$$-\frac{dN_A}{dt} = \pi d_c^2 k C_A^n \qquad \textbf{Equation 23}$$

This relation can be rewritten in terms of a volumetric heterogeneous reaction rate that can be implemented into the CFD of 1D code:

$$R^H = -\frac{1}{V}\frac{dN_A}{dt} = \frac{6}{d_g}\alpha_s k C_A = \frac{6}{d_g}\alpha_s k\left(\frac{x_A \rho_g}{M_A}\right) \qquad \textbf{Equation 24}$$

Equation 24 is formulated on the assumption that the reaction takes place at an equal rate on all the grains inside the particle. It is also assumed that there is no shrinkage of the unreacted core since a catalytic reaction was simulated. A first order reaction was simulated.

The hypothetical reaction rate constant in Equation 25 was implemented. Both the pre-exponential factor and the activation energy are representative of real materials used in fluidized bed reactor processes such as chemical looping combustion.

$$k = 0.1e^{(-100000/RT)} \qquad \textbf{Equation 25}$$

5 Methods

The results and subsequent analysis was based on a four factor central composite design [28]. This is a form of experimental design where the response of specific dependent variables to changes in various independent variables can be easily assessed, statistically quantified and visualized. The four independent variables, henceforth called factors, considered in the design were specified over five levels as follows:

- Gas flow rate (U). This factor was varied between 0.2 m/s and 1 m/s in 0.2 m/s intervals. These velocities produced fluidization falling in the lower to central regions of the bubbling fluidization regime. Lower fluidization velocities are expected to increase reactor performance (defined as the degree of gas conversion achieved) due to an increase in the gas residence time.

- Static bed height (H). The initial height of the bed was also varied between 0.2 and 1 m in 0.2 m intervals. This was chosen to facilitate direct comparison to the effect of gas flow rate. Similarly to the gas flow rate, an increase in the static bed height is expected to increase reactor performance by increasing the gas residence time.
- Reactor temperature (T). This factor was varied between 700 and 900°C in 50°C intervals. When implemented into Equation 25, this resulted in a factor 8.2 increase in the reaction rate constant which will increase reactor performance.
- Particle diameter (d). This factor was varied between 200 and 600 µm in 100 µm intervals and therefore represents typical Geldart B powder which is usually used in bubbling fluidized beds. The size of the particles used in fluidization has a large impact on the hydrodynamics, but also the reaction kinetics. Larger particle sizes are expected to decrease the expanded bed height, but also increase the rate of mass transfer from the bubble to the emulsion phase.

The effects of changes in these factors on reactor performance were evaluated by two dependent variables:

- Reactor performance expressed as $-\log(x_A)$ where x_A is the fraction of species A (reactant) exiting the reactor unreacted. In the 2D simulations, x_A was averaged both in time and space over the reactor outlet. This logarithmic performance measure was used to account for the first order nature of the reaction, where the reaction rate is directly proportional to the reactant concentration. This can be understood by acknowledging that an increase in conversion from 0% to 90% would require the same residence time as an increase in conversion from 90% to 99%, 99 to 99.9% and so forth. Due to the species A concentration being 10 times lower at 90% conversion than at 0% conversion, the

reaction rate is also 10 times lower. Hence, if all other influential factors are kept constant, achieving 9% extra conversion from 90% requires the same amount of gas residence time as achieving 90% extra conversion from 0%. Considering these numbers on a log-scale linearizes the conversion according to the gas residence time required. E.g. for 0% conversion $-\log(1)=0$, for 90% conversion $-\log(0.1)=1$, for 99% conversion $-\log(0.01)=2$, for 99.9% conversion $-\log(0.001)=3$, and so forth.

- Expanded bed height. This is directly calculated in the 1D model and was derived from time averaged data collected in the CFD model. The mean bed height was assumed to be located at a solids volume fraction value (averaged over time and cross-stream space) of 0.05.

The central composite design was run for the CFD (2D modelling) and subsequently for a number of different setups of the 1D model. Each completion of the central composite design required 26 simulation experiments, filling the four dimensional parameter space with reactor performance data as predicted by the particular model setup used. This facilitated a direct and easily quantifiable comparison between the performance of these different modelling approaches. Results presented and discussed below will mostly focus on quantifying the differences between the performance of the CFD model and various formulations of the 1D model.

The differences between CFD and 1D modelling were quantified and visualised by subtracting the 1D results from the CFD results for each of the 26 runs completed in every central composite design. This provided very informative trends on how the different modelling approaches differ in predicting system responses to changes in each of the four factors investigated.

Results will primarily be displayed in two ways: an analysis of variance (ANOVA) and response surfaces of dependent variables to changes in various factors. The ANOVA will be used to identify the most significant factors in the design (i.e. the factors where the different modelling methodologies give significantly different predictions).

The significance of factors will be defined by the p-value which is an indication of the probability of a repeated experiment to show the opposite response to that which is predicted by the model. If this value becomes small $\left(p < 0.05\right)$, the effect is said to be significant because the probability of it showing the opposite of the predicted response is sufficiently small. A value of $p < 0.01$ is generally regarded as highly significant. The p-value is calculated from the F-test. The F-test weighs the amount of explained variance in the design against the amount of unexplained variance (experimental error, rounding error, averaging error, data not fitting the second order model etc.). This ratio can then be evaluated as a p-value to decide whether the variance is caused by a significant effect (explained variance) or is simply random (unexplained variance).

The relative variance explained by each factor will also be given as the percentage of the total sum of squares (SS). The total sum of squares is the sum of all the squared distances between experimental points and the mean. A larger total sum of squares implies that experimental observations are scattered wide around the mean and there is a lot of variance in the design. This measure will give an indication of the importance of significant effects relative to each other.

Once the significant effects are identified in this way, the difference between CFD and 1D will be plotted on a response surface as a function of these highly significant factors in order to gain an understanding of the nature of various differences between the modelling methodologies.

6 Results and discussion

6.1 The CFD results

The CFD results will be used as the baseline in this work. Due to the much more fundamental nature of these simulations, it is assumed that CFD results are more accurate than those achieved with the 1D model and that any differences between CFD and 1D result from inaccurate closures used in the 1D approach.

In order to form a good understanding of the system in question therefore, the reactor performance as predicted by the CFD model first has to be analysed. The ANOVA for the CFD predictions of reactor performance $\left(-\log\left(x_A\right)\right)$ and expanded bed height are given in Table 3.

Linear, Quadratic and interaction effects are reported. A significant linear effect implies that reactor performance increases or decreases linearly with changes in the specific factor. If a significant quadratic effect is present, this implies that the response is curved (not simply a straight line). A significant interaction effect occurs when the reactor performance changes significantly when two factors are changed simultaneously.

Table 3: ANOVA table summarizing predictions by the CFD model. Significant factors are shown in bold, while highly significant factors are shown in bold italics. The factors are denoted by U (fluidization velocity), H (static bed height), T (reactor temperature) and d (particle diameter). Different effects are indicated by L (linear), Q (quadratic) and by (interaction).

Effect	Performance		Bed height	
	SS (%)	p-value	SS (%)	p-value
U(L)	***34,76***	***0,0000***	***20.17***	***0.0000***
U(Q)	**6,35**	**0,0107**	**0.08**	**0.0150**
H(L)	***8,40***	***0,0047***	***68.87***	***0.0000***
H(Q)	0,18	0,6145	0.03	0.0838
T(L)	***16,80***	***0,0004***	0.02	0.1546
T(Q)	0,43	0,4397	0.01	0.2375
d(L)	***11,90***	***0,0015***	***9.91***	***0.0000***
d(Q)	0,09	0,7198	**0.07**	**0.0221**
U(L) by H(L)	1,05	0,2385	***0.39***	***0.0000***
U(L) by T(L)	1,76	0,1342	0.00	0.7609
U(L) by d(L)	3,08	0,0558	0.00	0.5453
H(L) by T(L)	0,55	0,3854	0.01	0.2379
H(L) by d(L)	1,48	0,1668	***0.20***	***0.0007***
T(L) by d(L)	1,98	0,1150	0.00	0.7609
Error	7,42		0.10	
Total	100.00		100.00	

Table 3 shows highly significant linear effects $(p < 0.01)$ of all the factors in question as well as a significant quadratic effect for the fluidization velocity when looking at reactor performance. These results are very much the same as those observed in [29] and only the most important insights will be summarized here.

The effect of fluidization velocity was much larger than that of the static bed height, even though the ratio between low and high values of these factors was identical (The lowest level investigated was 0.2 and the highest level was 1.0 for both factors). This is due to the bubble size and resulting quality of gas-solid contact. At lower fluidization velocities, the bubble size becomes small and increases the quality of gas solid contact which causes an increase in conversion on top of that caused by the longer gas residence time. For taller beds, however, the bubble size grows with the height of the bed, thereby decreasing the degree of gas-solid contact and subtracting from the positive effect of the longer gas residence time.

Temperature had a significantly larger effect than the static bed height, but the effect was also significantly smaller than that of the fluidization velocity. Recall that the reaction rate increased by a factor of 8.2 from the lowest to the highest temperature investigated, which is higher than the ratio of 5 for the static bed height and the fluidization velocity. This is an indication that the mass transfer effect caused by the bubble size is more important than the reaction rate effect of the temperature. The effect of temperature was also decreased by an ever increasing relative strength of the mass transfer limitation as the temperature was increased. This is emphasized by the absence of a significant quadratic effect of temperature which would have been present if reactor performance increased exponentially (not just linearly as in this case) with the reaction rate.

The effect of particle size was not studied in [29] and it is interesting to observe such a large impact on reactor performance. Table 3 indicates that this factor explains more variance than the

static bed height. The effect of particle size will therefore be investigated further with the aid of Figure 3.

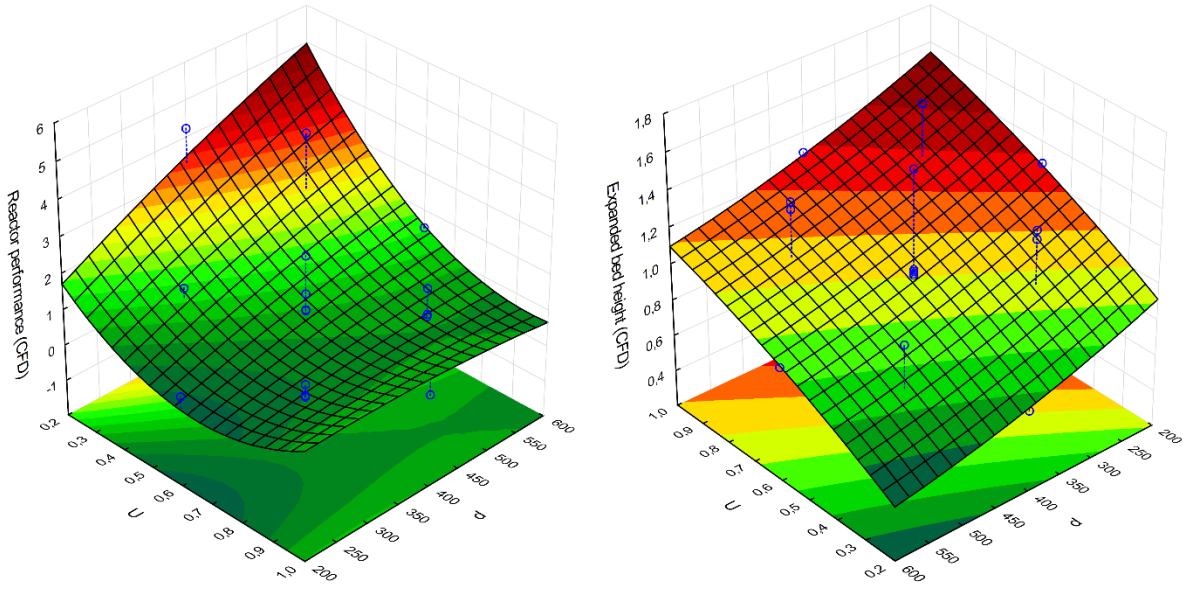

Figure 3: Response surfaces of reactor performance $\left(-\log\left(x_A\right)\right)$ and expanded bed height (m) to changes in fluidization velocity and particle diameter.

It is shown that an increase in particle size increases reactor performance, especially at lower fluidization velocities. This is interesting to observe, since it is also clear that an increase in particle size causes a significantly shorter bed, thereby decreasing the gas residence time. It can therefore be concluded that, for larger particle sizes, the positive effect of greater bubble-to-emulsion mass transfer outweighs the negative effect of reduced gas residence time, especially towards lower fluidization velocities. At higher fluidization velocities, these two effects seem to balance each other out and no visible effect of particle size is observed. This also offers an explanation for the interaction effect between fluidization velocity and particle size observed in Table 3 which is just above the 0.05 significance criterion.

It is important to note that increases in particle size only had such a strong positive effect on the reactor performance because of the reaction kinetic model implemented. Since the reaction was assumed to take place on constant sized grains within each particle, the reaction rate was

independent of the actual particle size. If the reaction was assumed to take place on the surface of the particles instead of the grains inside the particle, however, it is likely that an increase in particle size would decrease reactor performance because the volumetric reaction rate given in Equation 24 would then be inversely proportional to the particle size. In this case, the negative effect that larger particle sizes have on the reaction rate might overwhelm the positive bubble-to-emulsion mass transfer effect discussed in this section.

6.2 Simulation experiment 1: CFD versus the standard STP model

This section will use the STP model in exactly the same way as it is presented in the literature. The formulations for the bubble size and the bubble to emulsion mass transfer used for this paragraph are as described in Section 4.1.2. The ANOVA table for this case is given in Table 4.

.

Table 4: ANOVA table summarizing differences between CFD and the standard STP model. Significant factors are shown in bold, while highly significant factors are shown in bold italics. The factors are denoted by U (fluidization velocity), H (static bed height), T (reactor temperature) and d (particle diameter). Different effects are indicated by L (linear), Q (quadratic) and by (interaction).

Effect	Performance		Bed height	
	SS (%)	p-value	SS (%)	p-value
U(L)	**11,84**	**0,0143**	***8,86***	***0,0000***
U(Q)	1,61	0,3070	0,17	0,1893
H(L)	**7,48**	**0,0414**	***5,04***	***0,0000***
H(Q)	0,18	0,7237	0,14	0,2292
T(L)	***17,87***	***0,0044***	0,24	0,1230
T(Q)	4,86	0,0898	0,20	0,1587
d(L)	**15,48**	**0,0068**	***81,85***	***0,0000***
d(Q)	0,35	0,6290	0,28	0,1009
U(L) by H(L)	2,84	0,1827	**0,60**	**0,0233**
U(L) by T(L)	1,76	0,2865	0,01	0,7395
U(L) by d(L)	**7,26**	**0,0440**	0,30	0,0878
H(L) by T(L)	2,03	0,2543	0,16	0,1998
H(L) by d(L)	3,84	0,1265	**0,71**	**0,0153**
T(L) by d(L)	3,44	0,1458	0,01	0,7395
Error	15,45		0,95	
Total	100,00		100,00	

A quick and holistic measure of the performance of the 1D model in comparison to the CFD is the ratio of the total sums of squares from the design where the 1D model results were subtracted from the CFD (this section) and the design with only the CFD model (Section 6.1). If the 1D model reproduced the CFD results perfectly, there would be no variance in Table 4 since all points in the design would have exactly the same value as the mean (zero). Naturally, such a perfect fit cannot be realistically expected and there will always be some difference between the CFD and the 1D models as indicated by the variance in Table 4. If the 1D model reproduced the CFD results reasonably, however, the total amount of variance in Table 4 should be significantly less than the variance in Table 3.

The total sum of squares for reactor performance calculated with CFD was 26.67. When the STP 1D model results were subtracted, the variance reduced to 3.56. The ratio between these quantities is 0.1336, implying that the 1D model failed to account for only 13.36% of the variance within the results produced by the CFD. This is very satisfactory performance. Similarly, when looking at the expanded bed height, the same procedure gives the amount of variance not captured by the 1D model as 8.88%.

Table 4 can now be consulted to identify the factors where the CFD and 1D modelling approaches do not match well. For reactor performance, significant differences are observed for all factors. The particle diameter also features in a significant interaction effect with the fluidization velocity. When looking at the expanded bed height, it is clear that the vast majority of the difference between the CFD and 1D predictions lies in predicting the effect of changing particle diameter. These effects are studied further in Figure 4 and Figure 5.

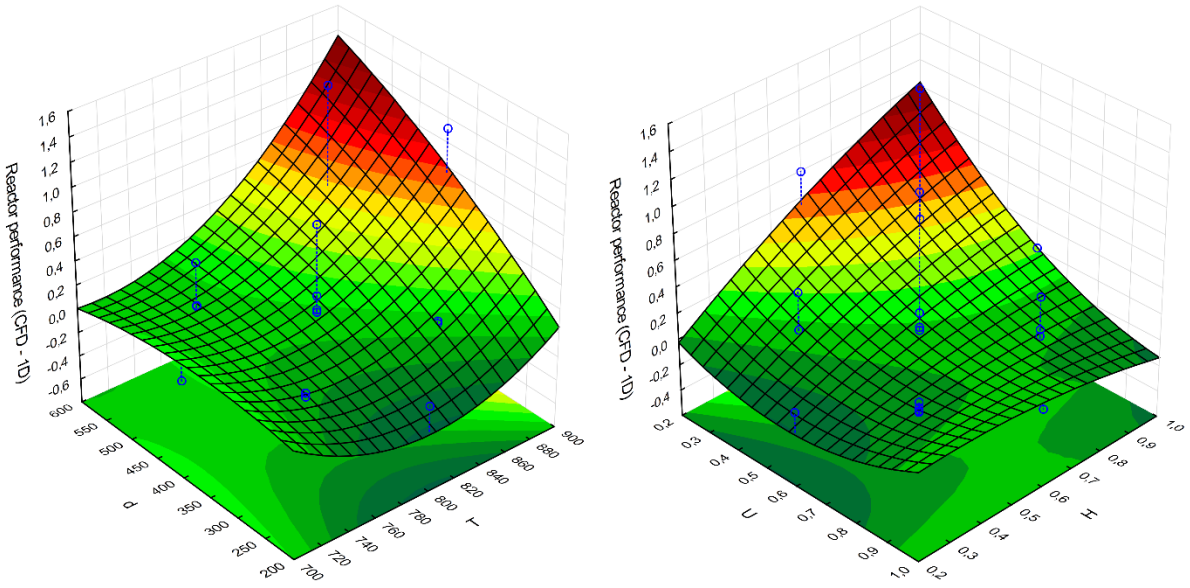

Figure 4: Response surfaces of reactor performance $\left(-\log\left(x_A\right)\right)$ to changes in all the independent variables.

When looking at reactor performance (Figure 4), it is clear that the CFD predicts significantly better reactor performance than the 1D model at higher temperatures, larger particle sizes, lower fluidization velocities and higher bed heights. The effect of temperature is likely to be caused by the standard STP 1D model not including any solids in the bubble itself. These solids inside the bubble start to significantly contribute to the reaction when the temperature becomes high and the bubble-to-emulsion mass transfer starts limiting the reactive contribution of the solids in the emulsion. The responses to changes in fluidization velocity and bed height simply imply that, at lower fluidization velocities and higher bed heights, gas residence times are longer, giving this error more time to accumulate.

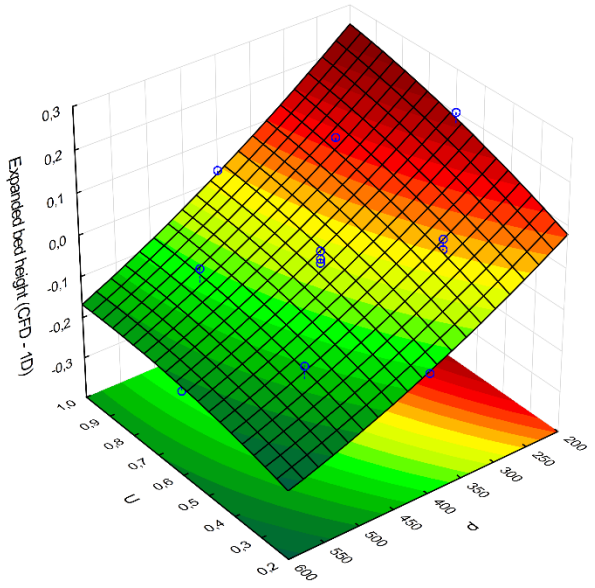

Figure 5: Response surface of expanded bed height (m) with changes in fluidization velocity and particle diameter.

The effect of the particle size implies that the CFD predicts a faster increase in bubble-to-emulsion mass transfer with an increase in particle size than the 1D model. This is further emphasized by looking at the response of the expanded bed height to changes in particle size (Figure 5). It is shown that the CFD predicts much shorter bed heights than the 1D model when the particle size is increased. This means that, despite significantly shorter gas residence times, the CFD model still predicts significantly better reactor performance when using larger particles. These findings raise question marks about the formulation of the bed expansion and the bubble-to-emulsion mass transfer models used in the 1D approach. If the CFD results are accurate, these models seem to be behaving inaccurately with changes in the particle size. Further study is recommended.

6.3 Simulation experiment 2: Alternative bubble size model

The bubble size model is a very important component in the 1D model. It has a direct influence on the bubble-to-emulsion mass transfer rate, the bubble velocity and the bubble fraction. These

factors greatly influence the predicted reactor performance and good performance of the bubble size model is therefore central to the accuracy of the 1D model.

In order to test this effect, a different bubble size model than the one used in Section 6.2 was implemented (Equation 6). This bubble size model predicted much smaller bubbles. In fact, these bubbles were so small close to the inlet that the predicted bubble velocity (Equation 8) was slower than the injection velocity of gas. This is of course unphysical. Therefore, a constant bubble size, calculated at the centre of the bed, was used for the new bubble size model. The ANOVA is given in Table 5.

.

Table 5: ANOVA table summarizing differences between CFD and the standard STP model with the alternative bubble size formulation. Significant factors are shown in bold, while highly significant factors are shown in bold italics. The factors are denoted by U (fluidization velocity), H (static bed height), T (reactor temperature) and d (particle diameter). Different effects are indicated by L (linear), Q (quadratic) and by (interaction).

Effect	Performance		Bed height	
	SS (%)	p-value	SS (%)	p-value
U(L)	**6,06**	**0,0121**	***39,10***	***0,0000***
U(Q)	0,18	0,6119	***0,47***	***0,0045***
H(L)	***10,27***	***0,0025***	***6,91***	***0,0000***
H(Q)	0,15	0,6513	0,01	0,6010
T(L)	***48,83***	***0,0000***	0,10	0,1350
T(Q)	0,65	0,3456	0,07	0,1978
d(L)	***17,88***	***0,0003***	***50,68***	***0,0000***
d(Q)	0,00	0,9348	0,01	0,5990
U(L) by H(L)	0,10	0,7013	***0,79***	***0,0007***
U(L) by T(L)	0,45	0,4302	0,00	0,7481
U(L) by d(L)	**5,77**	**0,0137**	***1,23***	***0,0001***
H(L) by T(L)	0,16	0,6319	0,06	0,2146
H(L) by d(L)	0,86	0,2835	0,01	0,5598
T(L) by d(L)	0,56	0,3815	0,00	0,7481
Error	7,41		0,40	
Total	100,00		100,00	

This model produced poorer results than the standard bubble size model (eq. 8). The overall performance measure of the degree of unexplained variance increased from 13.36% in Section 6.2 to 15.03% for reactor performance and from 8.88% to 22.41% of expanded bed height. For reactor performance, it can be seen that the effect of temperature is now even more pronounced with the effect of particle diameter being next in line. In the case of the expanded bed height, the effect of particle diameter is now joined by the effect of fluidization velocity. These effects will be examined more closely in Figure 6.

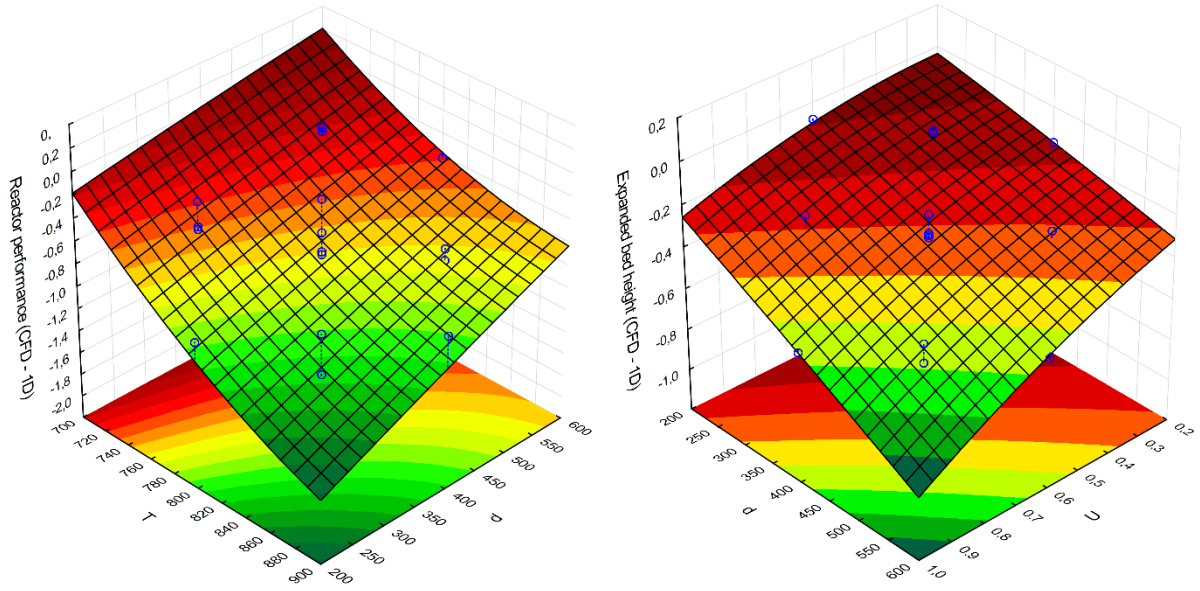

Figure 6: Response surfaces of reactor performance $\left(-\log\left(x_A\right)\right)$ and expanded bed height (m) to changes in significant factors.

The first observation from Figure 6 is that the 1D model with this bubble size formulation consistently over-predicts the reactor performance and the expanded bed height. This is deduced from the negative values of the CFD – 1D performance measures. The smaller bubble sizes predicted by this model lead to overestimations of the bubble-to-emulsion mass transfer, causing better reactor performance. Similarly, the smaller bubbles are modelled to rise slower, thus causing a greater void fraction and a larger bed expansion.

It is seen that the over-prediction of reactor performance worsens as the temperature and the reactor height is increased. This is a direct result of the over-prediction of the mass transfer coefficient, weakening the mass transfer limitation. In the absence of a strong mass transfer limitation, increases in temperature have a very large effect on reactor performance as can be seen in Figure 6.

For the expanded bed height, a similar trend to that seen in Figure 4 is visible for the particle diameter. The large effect of fluidization velocity is also evident though and indicates that the error worsens when more gas (and thereby more bubbles) is injected. The bubble size model is thus identified as a crucial constituent of the 1D modelling approach.

The analysis in the following paragraphs will be continued by using the standard bubble size model (Equation 7), as it showed the closest match to CFD.

6.4 Simulation experiment 3: Mass transfer formulations

The importance of the bubble-to-emulsion mass transfer formulation was emphasized by the significant effect of the bubble size model used. Aside from the bubble size model, there also are a number of other constituents to the mass transfer description. These will be discussed in this section.

Four options will be evaluated: the standard formulation implemented in Section 6.2 (Equation 11), only the convective term of this equation (first term of Equation 11), the inclusion of an additional cloud resistance (the full system of Equation 10, Equation 11 and Equation 12) and an alternative formulation (Equation 13). These formulations have no impact on the expanded bed height, so only the reactor performance will be reported and discussed. The ANOVA is given in Table 6.

Table 6: ANOVA table summarizing differences in reactor performance between CFD and the 1D model run with different mass transfer descriptions. Significant factors are shown in bold, while highly significant factors are shown in bold italics. The factors are denoted by U (fluidization velocity), H (static bed height), T (reactor temperature) and d (particle diameter). Different effects are indicated by L (linear), Q (quadratic) and by (interaction).

Effect	Standard		Only convection		Cloud resistance		Alternative	
	SS (%)	p-value	SS (%)	p-value	SS (%)	p-value	SS (%)	p-value
U(L)	**11,84**	**0,0143**	***24,05***	***0,0006***	***25,37***	***0,0001***	***20,08***	***0,0007***
U(Q)	1,61	0,3070	3,91	0,0826	**4,24**	**0,0282**	3,23	0,0866
H(L)	**7,48**	**0,0414**	**10,27**	**0,0102**	***10,22***	***0,0024***	***9,84***	***0,0073***
H(Q)	0,18	0,7237	0,22	0,6622	0,16	0,6329	0,16	0,6795
T(L)	***17,87***	***0,0044***	***25,41***	***0,0005***	***20,69***	***0,0002***	***20,49***	***0,0006***
T(Q)	4,86	0,0898	3,03	0,1213	0,94	0,2594	2,08	0,1587
d(L)	**15,48**	**0,0068**	3,78	0,0874	***15,01***	***0,0006***	***14,17***	***0,0023***
d(Q)	0,35	0,6290	0,18	0,6915	0,10	0,7095	0,28	0,5873
U(L) by H(L)	2,84	0,1827	2,45	0,1591	1,46	0,1660	2,12	0,1552
U(L) by T(L)	1,76	0,2865	2,62	0,1466	2,07	0,1050	2,14	0,1536
U(L) by d(L)	**7,26**	**0,0440**	3,35	0,1052	**3,76**	**0,0366**	**4,67**	**0,0449**
H(L) by T(L)	2,03	0,2543	1,73	0,2302	0,89	0,2706	1,47	0,2306
H(L) by d(L)	3,84	0,1265	2,14	0,1856	2,25	0,0928	2,88	0,1029
T(L) by d(L)	3,44	0,1458	1,77	0,2253	2,90	0,0606	3,41	0,0793
Error	15,45		11,81		7,31		10,03	
Total	100,00		100,00		100,00		100,00	

Firstly, the percentage of CFD variance not captured by the 1D model will be compared. For the standard case, this was 13.7% as described in Section 6.2. For the case featuring only convection driven mass transfer, this value was 21.71%, for the case with cloud resistance, 60.78%, and for the alternative formulation, 30.04%.

From these results it is clear that the standard formulation gives the best results. It also appears that the molecular diffusion term in the mass transfer equation has a significant effect and should be included. The inclusion of the additional cloud resistance, however, creates big errors in the results. Using the alternative mass transfer formulation also produces relatively poor results.

The reasons for the deviations in these alternative formulations will now be discussed. When looking at the case with only convective mass transfer, the first interesting observation is that the effect of particle size now seems to be adequately captured. This improvement is due to the mass transfer now being directly proportional to the minimum fluidization velocity which increases with particle size (the diffusive part of the mass transfer coefficient is independent of particle size). This makes the rate of mass transfer a stronger function of the particle size.

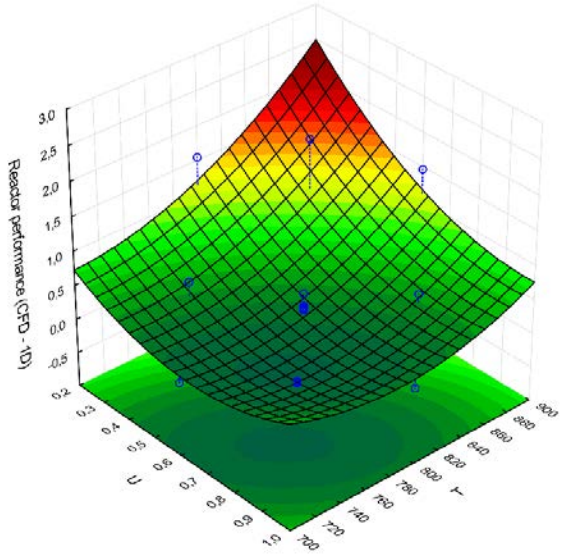

Figure 7: Response surface of reactor performance $\left(-\log\left(x_A\right)\right)$ in the case of only convective bubble-to-emulsion mass transfer.

The first observation from Figure 7 is that the 1D model now largely under-predicts reactor performance. This is due to the negligence of the diffusive mass transfer coefficient reducing the bubble-to-emulsion mass transfer.

Since this mass transfer is now under predicted, the mass transfer resistance becomes stronger and at higher temperatures, large under-predictions of the reactor performance in comparison with CFD are observed. Reactor performance at such high temperatures is mostly mass transfer controlled, implying that any error in the mass transfer description will be exaggerated. At lower temperatures, on the other hand, this is not the case and predictions are adequate. The effects of fluidization velocity and static bed height again show that greater gas residence times simply allow this error to compound.

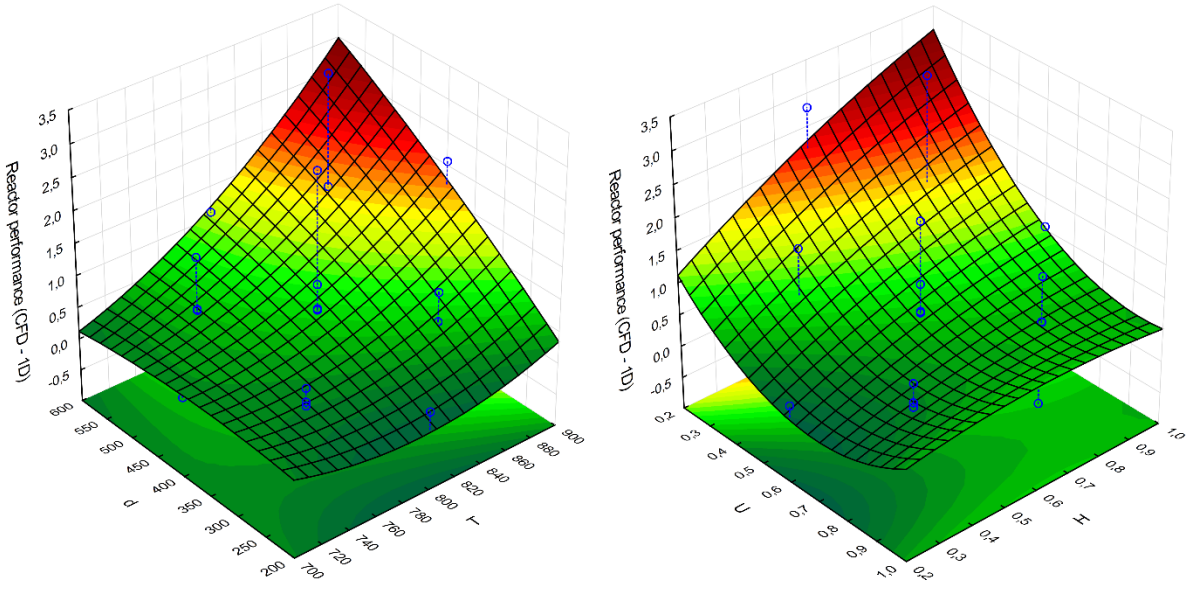

Figure 8: Response surfaces of reactor performance $\left(-\log\left(x_A\right)\right)$ in the case of an additional cloud mass transfer resistance.

When considering the addition of the cloud resistance, Figure 8 shows very similar trends to Figure 4, only significantly exaggerated. The same conclusions are valid for this case also. The only difference is the inclusion of a strong additional diffusion resistance, significantly strengthening the mass transfer resistance. This created significant under-predictions of reactor

performance throughout the design. The assumption of a significant cloud diffusion resistance is therefore not valid in this case.

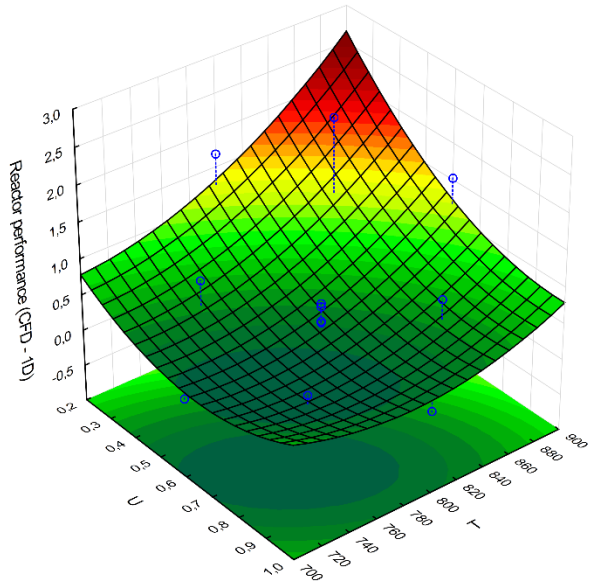

Figure 9: Response surface of reactor performance $\left(-\log\left(x_A\right)\right)$ using the alternative mass transfer formulation.

When using the alternative bubble-to-emulsion mass transfer coefficient, Figure 9 shows almost identical behaviour in response to changes in the two most significant factors (fluidization velocity and temperature) to that observed in Figure 7. The same conclusions are valid. The biggest difference between this case and the case with convection only mass transfer is that a significant effect of the particle size is again visible in Table 6, implying that the mass transfer rate does not increase sufficiently with increases in particle size.

More insight with regards to the response of the different mass transfer coefficient formulations to the particle size change can be gained by analysing the number of transfer units, NTU (Equation 26), for different cases. The results are summarized in Figure 10.

$$NTU = \frac{K_{be} H}{U_b} \qquad \textbf{Equation 26}$$

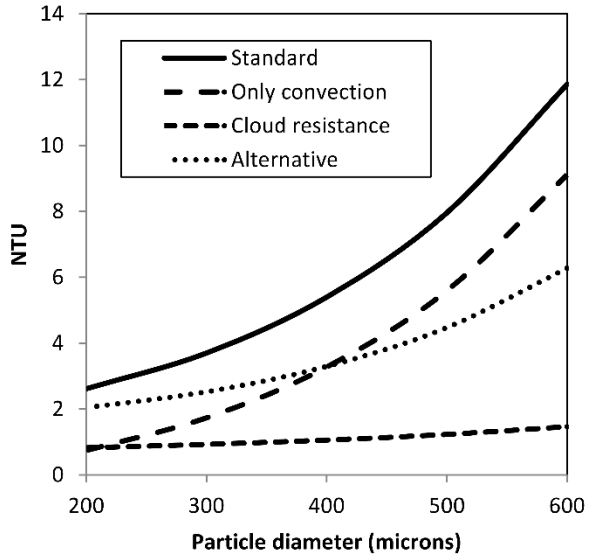

Figure 10: The number of transfer units (NTU) as a function of particle size for the four different mass transfer descriptions considered for a fluidization velocity of 0.6 m/s and a static bed height of 0.6 m.

Figure 10 shows a large degree of variation between the different mass transfer descriptions considered. It can be seen that the standard and the convection only mass transfer descriptions show an identical response to changes in particle size because the diffusive part of this description (second term in Equation 11) is independent of particle size. However, this constant addition of the diffusion resistance is shown to be highly significant, especially at smaller particle sizes where it is the primary influence on mass transfer.

Inclusion of the cloud resistance is shown to drastically increase the mass transfer resistance and thereby greatly reduce the number of transfer units. The cloud resistance (Equation 12) is also independent of particle size and is much more significant than the standard formulation (Equation 11). Therefore, this mass transfer limitation is only weakly dependent on particle size.

Finally, when considering the alternative mass transfer formulation, it is clear that the convective part of this formulation is less dominant than that of the standard formulation. This is clear from the weaker response to changes in particle diameter and can also be deduced by comparing the

two terms in Equation 11 and Equation 13. It has been concluded that a greater dependency on particle size is sought from the mass transfer formulation and therefore this alternative formulation only worsens the solution.

6.5 Simulation experiment 4: Solids inside the bubble

A potential source of error in the formulation of the STP is the assumption that the bubbles are completely clean, i.e. they contain no solids which can react with the gas residing in the bubble phase. In order to test the impact of this assumption, a simple model for solids volume fraction inside the bubble was derived only as a function of reactor height from the CFD simulation for the case with the tallest static bed height (Equation 27).

$$\alpha_s = \begin{cases} 3410h^4 - 943.1h^3 + 93.14h^2 - 4.104h + 0.1662 & \text{if } h < 0.1 \\ -0.0424h + 0.0855 & \text{if } 0.1 \le h < 2 \\ 0 & \text{if } h \ge 2 \end{cases} \quad \textbf{Equation 27}$$

In reality, the solids volume fraction inside the bubble is likely to also be a function of the fluidization velocity and the particle size, but these effects were neglected in this initial test. The ANOVA for this case is given in Table 7.

Table 7: ANOVA table summarizing differences between CFD and the 1D model with the inclusion of solids in the bubble. Significant factors are shown in bold, while highly significant factors are shown in bold italics. The factors are denoted by U (fluidization velocity), H (static bed height), T (reactor temperature) and d (particle diameter). Different effects are indicated by L (linear), Q (quadratic) and by (interaction).

Effect	Performance		Bed height	
	SS (%)	p-value	SS (%)	p-value
U(L)	**9,94**	**0,0419**	***24,14***	***0,0000***
U(Q)	1,98	0,3265	0,12	0,2297
H(L)	4,98	0,1316	***1,22***	***0,0019***
H(Q)	0,10	0,8192	0,19	0,1351
T(L)	*4,15*	*0,1651*	0,20	0,1281
T(Q)	4,11	0,1669	0,16	0,1676
d(L)	***24,09***	***0,0043***	***71,24***	***0,0000***
d(Q)	0,46	0,6319	0,27	0,0852
U(L) by H(L)	2,91	0,2385	0,13	0,2064
U(L) by T(L)	1,32	0,4194	0,01	0,7433
U(L) by d(L)	**10,30**	**0,0389**	0,22	0,1125
H(L) by T(L)	1,55	0,3827	0,13	0,2061
H(L) by d(L)	5,24	0,1229	**0,68**	**0,0115**
T(L) by d(L)	4,78	0,1386	0,01	0,7433
Error	20,64		0,82	
Total	100,00		100,00	

The percentage of CFD variance not explained by the 1D model decreased from 13.34% to 9.48% for the reactor performance, but increased from 8.88% to 10.7% for the expanded bed height when the solids volume fraction was included in the bubble.

The improvement in the prediction of the reactor performance is mostly due to a better prediction of the effect of temperature. It can be seen that the highly significant temperature effect that was present in Table 4 has now effectively been removed. This is a direct effect of the solids present inside the bubble which cause strong increases in reaction rate as the temperature is increased since the gas experiences no mass transfer limitation to react with these solids. The highly significant effect of particle size is still present, however, reaffirming the notion that the 1D models need revision with respect to their dependence on particle size.

For the expanded bed height, Table 7 shows a substantial increase in the effect of fluidization velocity in comparison to that observed in Table 4. This is an indication that the solids volume fraction in the bubble should be a function of the fluidization velocity as well.

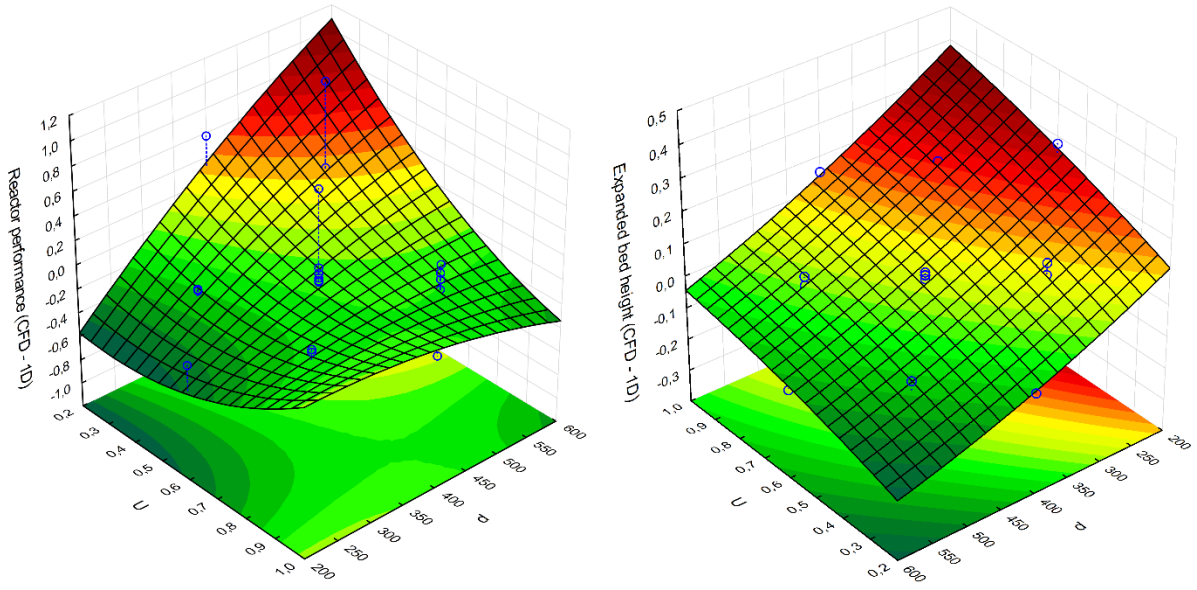

Figure 11: Response surfaces of reactor performance $\left(-\log\left(x_A\right)\right)$ and expanded bed height (m) to changes in fluidization velocity and particle diameter.

Figure 11 indicates that the reactor performance once again seems accurately predicted at high fluidization velocities, but when the fluidization velocity is decreased, and the gas residence time increased, the error resulting from the incorrect dependence of the mass transfer coefficient on the particle size becomes increasingly prominent.

Another important point regarding the reactor performance is that, quantitatively, the CFD and 1D results now seem to match very well. This can be deduced from the reactor performance response surface in Figure 11 where values are now roughly equally distributed around zero (where zero implies no difference between CFD and 1D). CFD predicted better reactor performance than the 1D model in all the other cases except for the alternative bubble size formulation where the 1D model greatly over-predicted reactor performance.

For the expanded bed height, the effect of the particle size is very similar to that observed in Figure 4. As for the effect of fluidization velocity, it is shown that the 1D model is increasingly over-predicting the bed height as the fluidization velocity is decreased. From CFD it was observed that the volume fraction of solids inside of the bubble indeed increases with a decrease in the fluidization velocity. This will decrease the overall voidage of the bed and thereby decrease the expanded bed height at lower fluidization velocities, serving to correct the trend shown in Figure 11. The derivation of a more representative model for solids volume fraction in the bubble is recommended for future study.

6.6 Detailed model comparisons

Axial data of several variables can be extracted from the 1D model to allow for more detailed comparisons to CFD than those discussed in the preceding sections. These comparisons were made for the centre-point of the central composite design (U = 0.6 m/s, H = 0.6 m, T = 800°C & d = 400 μm) and reported below.

6.6.1 Solids volume fraction

Figure 12 indicates that significant differences exist in the axial volume fraction distributions predicted by the two modelling approaches. Even though the current flow situation falls well within the bubbling fluidization regime, CFD results indicate a dense region of constant volume fraction (as would typically be associated with bubbling fluidization) only over the bottom two thirds of the vessel. The top third shows a rapid decrease in solids volume fraction, indicating that the nature of the bed changes when bubbles burst at the surface of the bed.

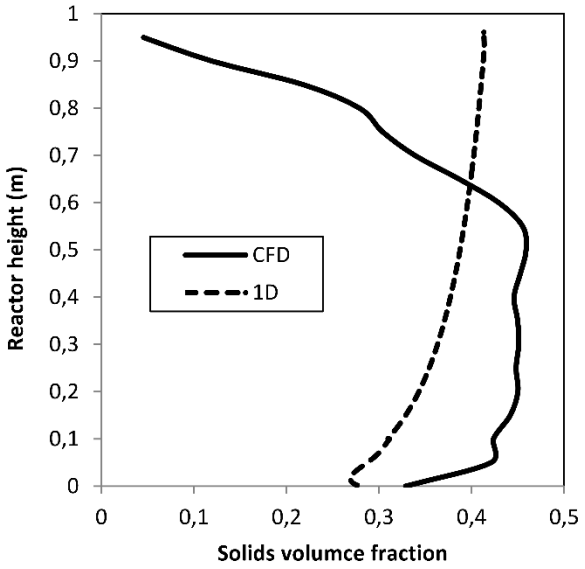

Figure 12: Axial volume fraction profiles predicted by the CDF and 1D approaches.

For the 1D approach, the entire bed was assumed to be under bubbling fluidization with bed material terminating abruptly at the surface of the expanded bed. The gradual increase in solids volume fraction along the height of the bed is a result of the bubble growth. According to the models used, larger bubbles rise faster and therefore create a lower local void fraction. CFD results, on the other hand, predict a constant volume fraction in the lower regions and a decreasing volume fraction in the upper regions, suggesting that these simple models have room for improvement in future studies.

However, since the 1D solids volume fraction is under-predicted in the lower regions and over-predicted in the upper regions of the vessel, the overall expanded bed height is predicted with reasonable accuracy.

6.6.2 Axial gas velocity

In the next two sections, a distinction is made between the bubble and emulsion phase. For the CFD simulations, this distinction was made by considering all regions with a solids volume fraction lower than a specific predefined value to be part of the bubble phase and all regions with a solids volume fraction greater than this value to be part of the emulsion phase. Axial superficial gas velocities occurring both above and below this solids volume fraction cut-off value were averaged separately in time and horizontal space according to Equation 21.

$$\frac{\sum_{x=x_L}^{x=x_R}\left(\sum_{t=t_0}^{t=t_{end}}\alpha_g v_g \Delta t\right)}{\sum_{x=x_L}^{x=x_R}\left(\sum_{t=t_0}^{t=t_{end}}\Delta t\right)} \qquad \textbf{Equation 28}$$

Here, x_L and x_R indicate the left-most and right-most cells while t_0 and t_{end} indicate the first and last timesteps of the time-averaging period. Different choices of the cut-off value were evaluated as displayed in Figure 13.

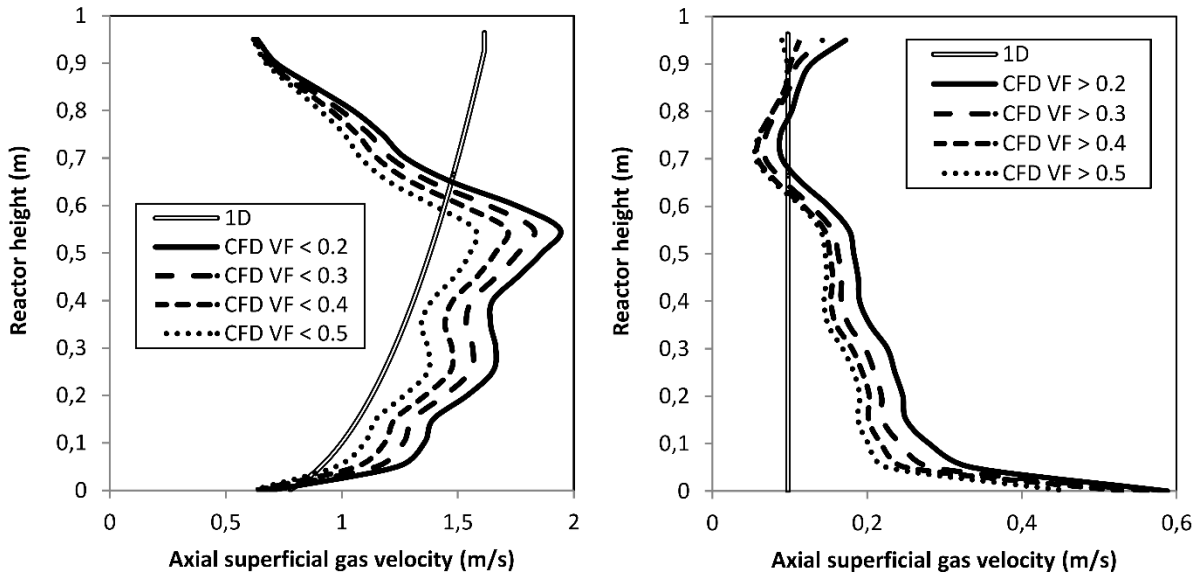

Figure 13: Axial superficial gas velocity profiles in the bubble (left) and emulsion (right) phases for different solids volume fraction (VF) cut-off points.

When looking at the bubble phase velocities in Figure 13, it can be seen that the CFD generally predicts higher bubble velocities in the lower regions and smaller bubble velocities in the upper regions in comparison to the 1D model. The bubble velocity trends in Figure 13 are very similar to the solids volume fraction trends in Figure 12. This confirms the inverse relationship between mean void fraction and bubble velocity used in the 1D modelling approach.

For the CFD results, it can be seen that the bubble velocity increases gradually in the lower regions of the bed while the solids volume fraction stays reasonably constant (Figure 12), thereby deviating somewhat from the expected inverse proportionality between void fraction and bubble velocity. For the emulsion phase, however, it can be seen that, in the lower regions, CFD predicts much higher velocities than the 1D model and this discrepancy gradually reduces along the height. Summing these two discrepancies would therefore result in a more constant overall gas velocity in the lower regions as would be suggested by Figure 12.

The faster gas velocities predicted by the CFD model in the emulsion phase imply that particles are in the process of being accelerated in the upwards direction by the rising gas in the lower

regions of the reactor. This feature can have a significant effect on reactor performance by allowing more gas to pass through the emulsion phase where the reaction occurs very rapidly. Figure 13 also shows that the volume fraction cut-off point between the bubble and emulsion phases has a significant impact on the results. For the bubble phase, the average axial superficial velocity decreases with an increase in the cut-off volume fraction since more cells containing larger amounts of solids (and therefore lower gas velocities) are included in the averaging process. A similar trend is visible for the emulsion phase where a higher cut-off point removes the contribution of cells containing less solids (and therefore larger gas velocities).

It can also be argued that the larger bubble velocity predicted by the CFD approach is a result of the relatively small system (ID = 28 cm) simulated. The close proximity of the walls implies that solids recirculation plays a very important role. Solids falling down the walls of the reactor force gas bubbles to slip rapidly up the centre of the vessel and thereby increases the overall gas slip velocity and the overall solids volume fraction. This might not be the case in larger vessels and is a topic recommended for future study.

6.6.3 Reacting gas concentrations

Axial profiles of reactant mass fractions in the bubble and emulsion phases are plotted in Figure 14 using the same criteria to distinguish between the bubble and emulsion phases. The first observation is that the CFD and 1D predictions of the gas concentrations in the bubble phase are virtually identical. This is very encouraging, since the vast majority of gas passes through the bubble phase and accurate predictions of this phase therefore leads to accurate predictions of overall reactor performance.

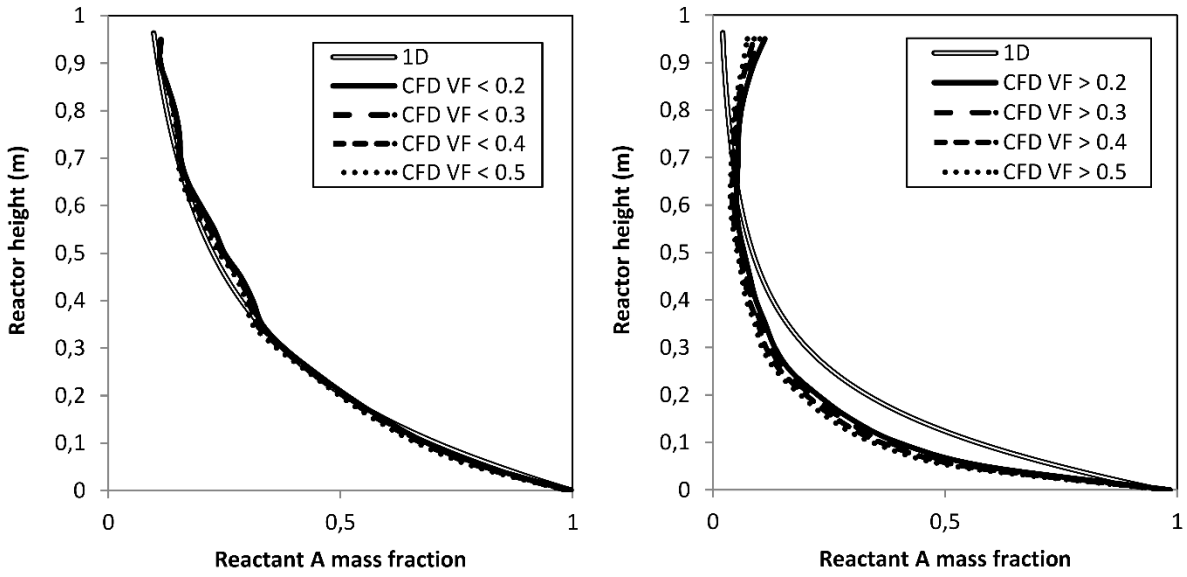

Figure 14: Axial profiles of the reactant A in the bubble (left) and emulsion (right) phases for different solids volume fraction (VF) cut-off points.

Larger discrepancies are shown in the emulsion phase. This is primarily due to the larger quantity of solids present in the lower regions of the CFD predictions (Figure 12). Due to this larger solids mass, the emulsion phase presents a greater surface area for reaction and the reactant is consumed at a greater rate. The lower reactant concentration in the emulsion phase also implies that mass transfer is faster in the CFD simulation (due to a larger concentration difference between bubble and emulsion), but the similar bubble reactant concentrations predicted by CFD and 1D imply that the greater bubble to emulsion mass transfer is compensated almost exactly by the greater bubble slip velocity (Figure 13). These two sources of error therefore serve to cancel each other out, leading to reasonably accurate predictions of overall reactor performance.

The solids volume fraction cut-off point between bubble and emulsion does not seem to have a significant impact on results, especially for the bubble phase. An interesting feature occurs towards the top of the reactor, however, where the reactant concentration in the emulsion phase seemingly increases with reactor height. This is due to the distinction between bubble and

emulsion becoming less distinct in the bubble burst region towards the top of the bed. Therefore, as the top of the bed is approached, the gas concentration in the bubble and emulsion will become similar.

6.6.4 Bubble size

The CFD bubble diameter predictions in Figure 15 were compiled by measuring the horizontal dimension of all bubbles in 10 volume fraction snapshots (similar to Figure 1) taken 0.5 s apart. It is clear that the CFD and 1D predictions of bubble diameter are quite similar even though the wide spread in CFD predicted bubble sizes towards the upper reactor regions might suggest a slightly lower mean size than that used in the 1D model.

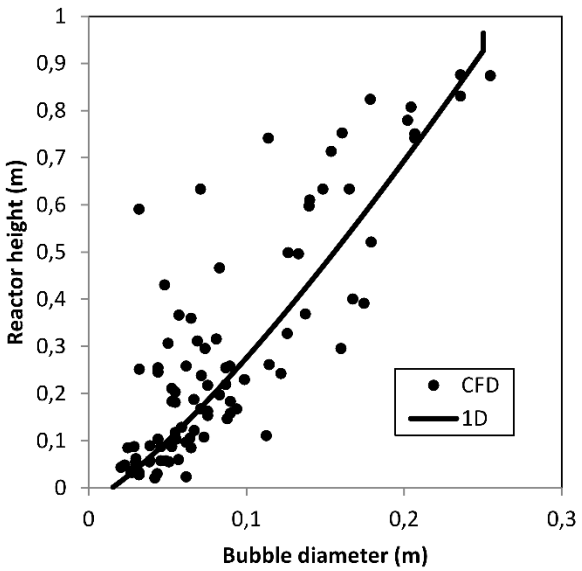

Figure 15: Axial comparisons of bubble diameter predictions by 1D and CFD.

Bubble size is a central parameter in the 1D modelling approach, influencing the mass transfer coefficient as well as the bubble rise velocity and subsequent bubble/emulsion phase distribution. It is therefore encouraging to see that the 1D and CFD approaches returned very similar predictions of this crucial parameter. This is seen as one of the primary reasons for the close match between CFD and 1D predictions of overall reactor performance.

7 Conclusions

A standard bubbling fluidized bed reactor was simulated both in 1D using a MATLAB code and in 2D using the CFD code, FLUENT 13.0. These models were tested and compared over a wide range of operating conditions in order to pinpoint any differences in the results produced. In general, the 1D model performed very well, explaining up to 90% of the variance present in the reactor performance predicted by the CFD model over widely varying fluidization velocities, bed heights, reaction temperatures and particle sizes.

Various setups of the 1D model were tested. The description of the mass transfer was found to be of critical importance. A number of different alternatives were evaluated to identify the most suitable candidate. The formulation of the bubble size model, forming a part of the mass transfer coefficient, was also found to have a significant effect on results.

In general, the predictions of the 1D model compared favourably to the CFD predictions for changes in the fluidization velocity and the bed height. For the standard 1D model formulation, the effect of changing the reaction temperature was not adequately captured because the 1D model assumes the bubble to be clean of all solids. In reality, a significant amount of solids are present in the bubble. These solids are then capable of directly reacting with the gas inside the bubble without being subject to the bubble-to-emulsion mass transfer limitation and exert an increasingly strong influence on reactor performance as the temperature (and thus the reaction rate) is increased. In order to account for this effect, a simple model for the solids volume fraction inside the bubble was added to the 1D model. This addition successfully removed the significant temperature effect.

The only variable where the 1D model could not match the CFD is the particle diameter. Results showed that the current formulations of the 1D model do not show a strong enough dependency on the particle size when it comes to the mass transfer coefficient and the bubble rise velocity.

The CFD results show that the reactor performance increases significantly more with an increase in particle diameter than predicted by the 1D model. Similarly, the CFD model shows that the expanded bed height decreases significantly more with an increase in the particle diameter than seen for the 1D model. Both these effects will require further research attention since, considering the wide range of particle sizes used in fluidized bed applications, they could lead to significant errors in model predictions.

More detailed comparisons of axial profiles of important flow variables derived form the 1D and CFD approaches revealed some significant differences in the two approaches. Axial distributions of mean void and superficial gas velocity were predicted differently by about 20%. Several possible reasons for this difference was identified and recommended for future research. Different inconsistencies between the modelling approaches tended to cancel out, however, leading to adequate overall reactor performance predictions.

8 Future work

Experiments are currently being conducted to validate the CFD models used in this work over a wide range of operating conditions. From this study, it seems that the effect of particle diameter will be especially important to capture correctly. Once the CFD model is validated, it can be safely used to upgrade the closure laws used in the 1D model and guarantee sufficient accuracy over a wide range of flow conditions. In this way, expensive and complex, but accurate CFD simulations can be used to formulate cheap and simple, but still sufficiently accurate 1D models that will be of great use to industry.

9 Acknowledgment

The authors would like to acknowledge the financial support received from the Research Council of Norway under the Flow@CLC grant.

10 References

[1] Kunii D, Levenspiel O. Fluidized reactor models.1. For bubbling beds of fine, intermediate and large particles. 2. For the lean phase - freeboard and fast fluidization. Industrial & Engineering Chemistry Research. 1990 Jul;29(7):1226-34.
[2] Davidson JF, Harrison, D., ed. Fluidized particles. New York 1963.
[3] Kunii D, Levenspiel, O., ed. Fluidization Engineering. Stoneham: Butherworth-Heinemann 1991.
[4] Werther J. Modelling and scale-up of industrial fluidized bed reactors. Chemical Engineering Science. 1980 1980;35(1-2):372-9.
[5] Grace JR. Generalized Models for Isothermal Fluidized Bed Reactors. In: Doraiswamy LK, editor. Recent Advances in the Engineering Analysis of Chemically Reacting Systems; 1984 1984; New Delhi, India: Wiley Eastern; 1984. p. 237.
[6] Faltsi-Saravelou O, Vasalos IA. FBSim: A model for fluidized bed simulation—I. Dynamic modeling of an adiabatic reacting system of small gas fluidized particles. Computers & Chemical Engineering. 1991;15(9):639-46.
[7] Faltsi-Saravelou O, Vasalos IA, Dimogiorgas G. FBSim: A model for fluidized bed simulation—II. Simulation of an industrial fluidized catalytic cracking regenerator. Computers & Chemical Engineering. 1991;15(9):647-56.
[8] Maroufi S, Khoshandam B, Kumar RV. Mathematical modelling of fluidized bed reactors for non-catalytic gas-solid reactions. Canadian Journal of Chemical Engineering. 2010 Dec;88(6):1034-43.
[9] Abad A, Adanez J, Garcia-Labiano F, de Diego LF, Gayan P. Modeling of the chemical-looping combustion of methane using a Cu-based oxygen-carrier. Combustion and Flame. 2010 Mar;157(3):602-15.
[10] Mostoufi N, Cui HP, Chaouki J. A comparison of two- and single-phase models for fluidized-bed reactors. Industrial & Engineering Chemistry Research. 2001 Nov;40(23):5526-32.
[11] Jafari R, Sotudeh-Gharebagh R, Mostoufi N. Performance of the wide-ranging models for fluidized bed reactors. Advanced Powder Technology. 2004;15(5):533-48.
[12] Thompson ML, Bi HT, Grace JR. A generalized bubbling turbulent fluidized-bed reactor model. Chemical Engineering Science. 1999 Jul;54(13-14):2175-85.
[13] Abba IA, Grace JR, Bi HT, Thompson ML. Spanning the flow regimes: Generic fluidized-bed reactor model. Aiche Journal. 2003 Jul;49(7):1838-48.
[14] Gidaspow D, Bezburuah R, Ding J. Hydrodynamics of Circulating Fluidized Beds, Kinetic Theory Approach. *7th Engineering Foundation Conference on Fluidization* 1992:75-82.
[15] Lun CKK, Savage SB, Jeffrey DJ, Chepurniy N. Kinetic Theories for Granular Flow: Inelastic Particles in Couette Flow and Slightly Inelastic Particles in a General Flow Field. Journal of Fluid Mechanics. 1984;140:223-56.
[16] Syamlal M, Rogers W, O'Brien TJ. MFIX Documentation: Volume 1, Theory Guide. Springfield: National Technical Information Service 1993.
[17] Taghipour F, Ellis N, Wong C. Experimental and computational study of gas-solid fluidized bed hydrodynamics. Chemical Engineering Science. 2005;60(24):6857-67.

[18] Grace JR. Contacting modes and behaviour classification of gas—solid and other two-phase suspensions. The Canadian Journal of Chemical Engineering. 1986;64(3):353-63.
[19] Cai P, Schiavetti M, Demichele G, Grazzini GC, Miccio M. Quantitative estimation of bubble size in PFBC. Powder Technology. 1994 Aug;80(2):99-109.
[20] Darton RC, Lanauze RD, Davidson JF, Harrison D. Bubble growth due to coalescence in fluidized beds. Transactions of the Institution of Chemical Engineers. 1977 1977;55(4):274-80.
[21] Sit SP, Grace JR. Interphase mass transfer in an aggregative fluidized bed. Chemical Engineering Science. 1978 1978;33(8):1115-22.
[22] Schaeffer DG. Instability in the Evolution Equations Describing Incompressible Granular Flow. Journal of Differential Equations. 1987;66:19-50.
[23] Ogawa SU, A.; Oshima, N. On the Equation of Fully Fluidized Granular Materials. Journal of Applied Mathematics and Physics. 1980;31:483.
[24] Patankar S. Numerical Heat Transfer and Fluid Flow: Hemisphere Publishing Corporation 1980.
[25] Leonard BP, Mokhtari S. ULTRA-SHARP Nonoscillatory Convection Schemes for High-Speed Steady Multidimensional Flow. NASA TM 1-2568 (ICOMP-90-12); 1990; NASA Lewis Research Center; 1990.
[26] Johnson PC, Jackson R. Frictional-Collisional Contitutive Relations for Granular Materials, with Application to Plane Shearing. Journal of Fluid Mechanics. 1987;176:67-93.
[27] Levenspiel O. Chemical Reaction Engineering. 3 ed: John Wiley & Sons 1999.
[28] Montgomery D. Design and Analysis of Experiments. 5 ed. New York: John Wiley and Sons 2001.
[29] Cloete S, Amini S. Mapping of the Operating Window of a Lab Scale Bubbling Fluidized Bed Reactor by CFD and Designed Experiments. *8th International Conference on CFD in the Oil & Gas, Metallurgical and Process Industries* Trondheim, Norway 2011.